Image Quality Degradation and Retrieval Errors Introduced by Registration and Interpolation of Multispectral Digital Images

Bradley G. Henderson, Christoph C. Borel, James Theiler, and Barham W. Smith

NIS-2, Mail Stop C323
Los Alamos National Laboratory
Los Alamos, NM 87545

ABSTRACT

Full utilization of multispectral data acquired by whiskbroom and pushbroom imagers requires that the individual channels be registered accurately. Poor registration introduces errors which can be significant, especially in high contrast areas such as boundaries between regions. We simulate the acquisition of multispectral imagery in order to estimate the errors that are introduced by co-registration of different channels and interpolation within the images. We compute the Modulation Transfer Function (MTF) and image quality degradation brought about by fractional pixel shifting and calculate errors in retrieved quantities (surface temperature and water vapor) that occur as a result of interpolation. We also present a method which might be used to estimate sensor platform motion for accurate registration of images acquired by a pushbroom scanner.

Keywords: Image Processing, Registration, Reconstruction, Linear Filtering

1 INTRODUCTION

Modern imaging devices used in remote sensing of earth and planetary surfaces are multi- and hyperspectral in design and thus acquire data at multiple wavelengths across the electromagnetic spectrum. Often times, these systems employ physically separated detectors (whiskbroom) or detector arrays (pushbroom) for each channel (e.g., Landsat, SPOT, AVHRR, MODIS, MISR, ...). Exploiting the multi-wavelength nature of the data requires that each spectral band be registered to all of the other bands so that corresponding pixels in the individual images represent the same point on the surface. In general, the bands are not registered due to imperfections in the optical system, telescope distortion, motion of the spacecraft, slew rate delays in readout electronics, etc. Pixel mis-registration can be a large source of error in areas of high contrast such as boundaries between materials or terrains. For certain applications, sub-pixel accuracy is desired when registering channels, which requires fractional pixel shifting, or, equivalently, interpolation. Interpolation introduces errors in radiometry and loss of resolution which must be understood and minimized in order to improve retrievals and also to evaluate the overall quality of the image.

Currently, we are developing an end-to-end simulation of the acquisition of multispectral imagery of the earth's surface for a particular system design (Smith et al., 1996). A schematic is shown in Fig. 1 which depicts the different Optical Transfer Functions (OTF) utilized in the simulation. In this study, we focus on one piece of

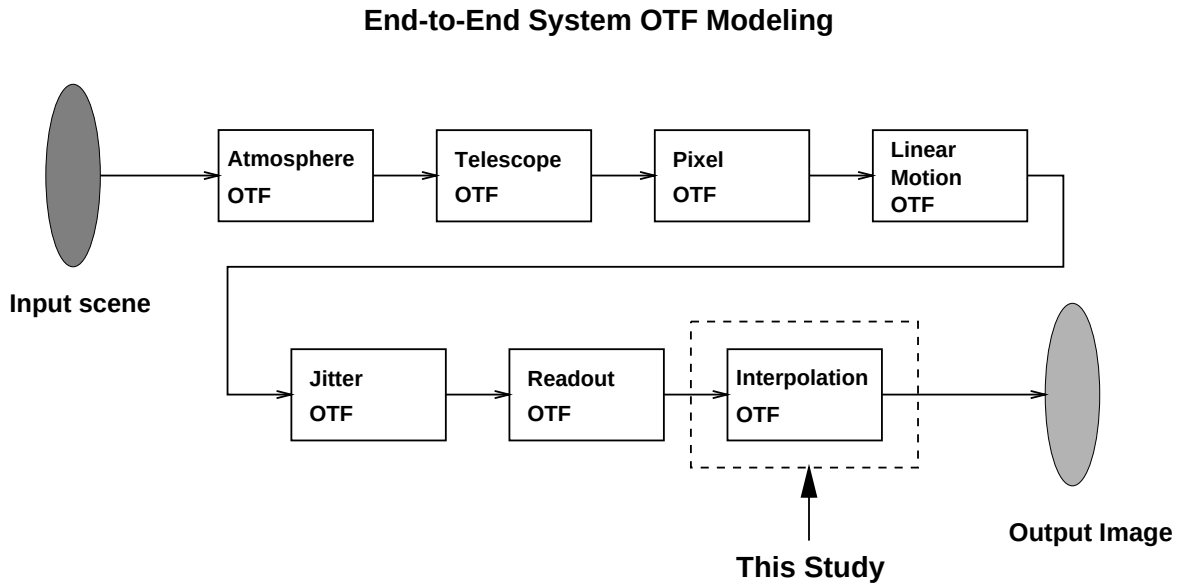

Figure 1: Schematic showing some of the different Optical Transfer Functions (OTF) used in an end-to-end simulation. This study concentrates on the interpolation OTF for registering multispectral digital images.

the system OTF, that of the interpolation required for registration of multispectral digital images. In the next section of the paper, we compute the Modulation Transfer Function (MTF = |OTF|) of fractional pixel shifting for various interpolation algorithms. In the following section, we compute the error caused by interpolation for retrieving surface temperature and water vapor from multispectral images. In the final section, we present a new method for registration of multispectral images acquired by a pushbroom imager.

2 MTF OF FRACTIONAL PIXEL SHIFTING

Image registration performed at sub-pixel accuracy requires interpolation, which degrades resolution and image quality. In practice, interpolation is carried out by fitting a continuous function to existing data points. However, interpolation is equivalent to convolving the data points with the appropriate kernel. Treating interpolation as a convolution operation is useful because analysis of the kernel allows one to evaluate the performance and accuracy of a given interpolation algorithm.

Kernels for three of the more commonly used interpolation algorithms are shown in Figs. 2a – 2c for linear and cubic convolution. The cubic convolution kernel is actually a one-parameter family of piecewise cubic polynomials (see Park and Schowengerdt, 1983) represented by

$$r(x) = \begin{cases} (\alpha+2)|x|^3 - (\alpha+3)|x|^2 + 1 & |x| < 1 \\ \alpha|x|^3 - 5\alpha|x|^2 + 8\alpha|x| - 4\alpha & 1 \le |x| < 2 \\ 0 & \text{otherwise.} \end{cases} \quad (1)$$

The parameter α has mathematical significance in that it gives the slope of the kernel at $x = 1$. Figs. 2b and 2c show the cubic convolution kernel for both $\alpha = -0.5$ and $\alpha = -1$, two of the more commonly used values. Viewed as a convolution process, interpolation acts as a low-pass filter and in effect smooths the data by suppressing the higher frequencies. The frequency response of the interpolator, i.e., the Modulation Transfer Function (MTF), is obtained by taking the amplitude of the Fourier transform of the kernel. For example, the MTF for linear

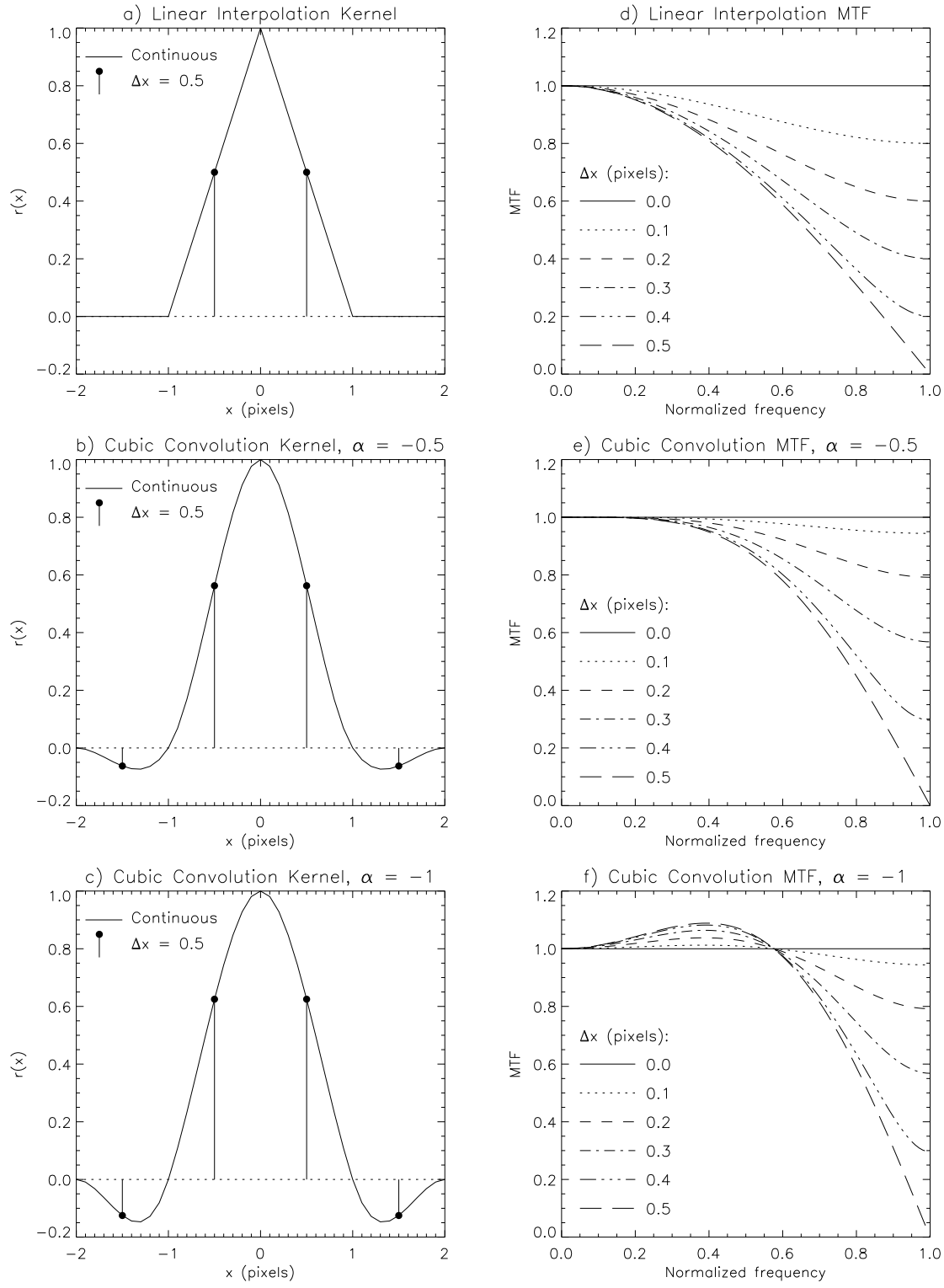

Figure 2: (a) – (c): Kernels for linear interpolation and cubic convolution ($\alpha = -0.5$ and $\alpha = -1$, see text for details). The solid line gives the kernel as a continuous function, whereas the posts show the sampled kernel for a fractional pixel shift (Δx) of 0.5. (d) – (f): Modulation Transfer Function (MTF) for each interpolation algorithm plotted for fractional shifts 0 – 0.5 pixel.

interpolation is given by

$$MTF_{lin-interp} = \text{sinc}^2\left(\pi \frac{f}{f_s}\right) \tag{2}$$

in which f is the spatial frequency and f_s is the sampling frequency (see Holst, 1995). However, a subtlety which is often ignored in this step is that fact that the MTF varies with fractional pixel shift within the scene. In other words, the farther the interpolant is from the original data points, the greater the error and the greater the loss in resolution. Figs. 2a – 2c show sampled kernels for a fractional pixel shift (Δx) of 0.5 for obtaining interpolated values half way between the original data points. The MTF for a fractional pixel shift of $\Delta x = 0.5$ is obtained by taking the amplitude of the Fourier transform of the *sampled* kernel. Figs. 2d – 2f show computed MTF's for the three kernels computed for fractional pixel shifts 0.0 – 0.5. Note that the MTF is a strong function of pixel shift. For shifts of 0.1 or smaller, the MTF stays near 1 for all frequencies. As the fractional pixel shift increases, the MTF falls significantly below unity, especially at the higher frequencies. This decrease in MTF gives rise to image quality degradation and loss of information which introduces errors into retrieval algorithms when registering multispectral images. In general, the MTF is higher for cubic convolution than for linear interpolation. The cubic convolution method is thus more capable of preserving the signal in high frequency areas such as the borders between terrains but can introduce ringing at sharp boundaries. In general, its use will minimize interpolation errors and will improve accuracy in quantities retrieved from registered multispectral images, as will be seen below.

3 ERRORS INTRODUCED TO RETRIEVAL ALGORITHMS BY REGISTRATION/INTERPOLATION

3.1 Introduction

The use of multiple bands for retrieving physical quantities from multispectral images necessitates the need for accurate registration. While some simpler retrievals such as vegetation index utilize as few as two bands, other more complicated retrievals will utilize 10 or more channels with varying viewing geometries. The task of registering the individual images becomes more complicated, thus increasing the potential for error. In this section, we examine the errors caused by registration for two quantities (surface temperature and water vapor) which utilize multiple bands in the retrieval algorithm.

3.2 Surface Temperature Retrieval

Many current and future remote sensing satellites will retrieve earth surface temperature by inverting infrared thermal emission measurements. Determining surface temperature is important for studies of the earth's energy budget and for monitoring global climate and climate change. There exist a number of techniques for computing surface temperature from IR emission measurements. Almost all of the more recent methods employ a multi-spectral technique and therefore require registration prior to temperature retrieval. When imaging scenes with large temperature contrasts (relative to the pixel size), sub-pixel accuracy is desired in the registration process, which requires interpolation. For our specific application, we are interested in determining the magnitude of the temperature retrieval error introduced by the interpolation of the spectral images used in the retrieval algorithm.

For this temperature retrieval simulation, we used the multi-spectral multi-angular technique developed by Tornow et al. (1994). This method uses a linear regression of radiances measured at five spectral channels in the mid- and long-wave IR taken at both nadir and 60° for a total of 10 measurements. The reader is referred to that reference for more detail. The off nadir looks used by this method require an additional registration step due to the different geometries in the two observations. The steps in the simulation are depicted in Fig. 3. The

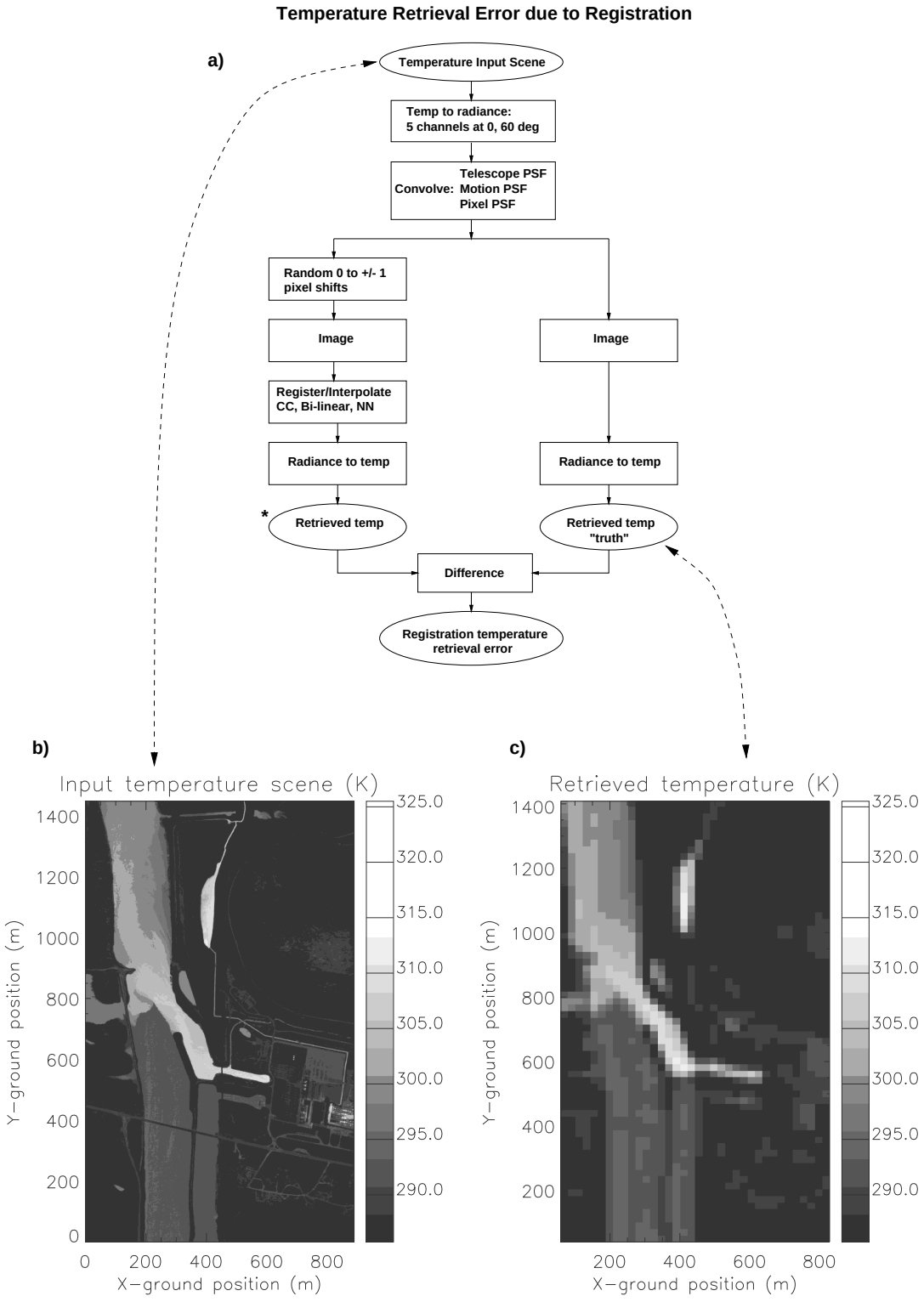

Figure 3: a) Flow chart showing the steps in the simulation. b) Input temperature scene. c) Temperature retrieved by the sensor with no included jitter. A "total" error compares the retrieved temperature (marked by a * above) to b), whereas the error just due to interpolation is given by comparison of * to c).

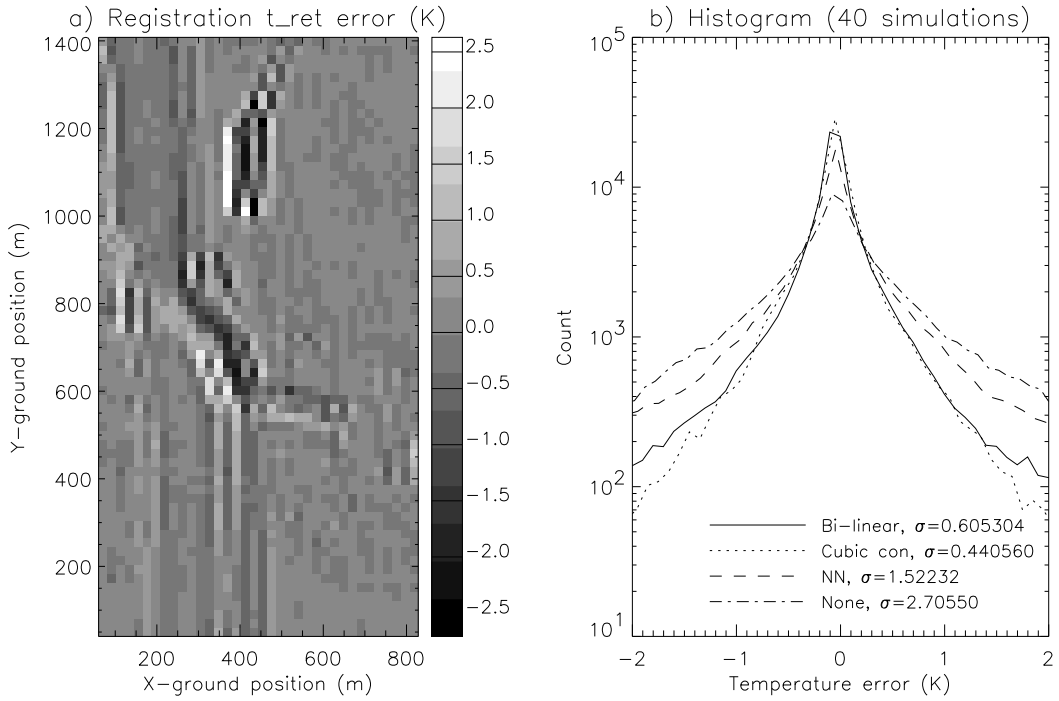

Figure 4: (a) Error in retrieved temperature due to registration (one trial). (b) Histogram of temperature error computed for 40 trials using different interpolation schemes, including bi-linear, cubic convolution ($\alpha = -1$), nearest neighbor, and none. The computed RMS error for each method is given at top.

simulation begins with an input temperature scene with resolution 10 times that of the sensor of interest. The temperature map is converted to top of atmosphere (TOA) radiances for 5 bands in the mid- and long-wave IR at look geometries of 0° and 60° using an algorithm based on MODTRAN (Berk et al., 1989). Those radiances are then blurred by the system MTF which, for this particular simulation, includes the effects of the optics, linear motion for a pushbroom scanner, and the pixel size. Those radiances are then imaged twice, once "perfectly" assuming uniform sensor motion during the imaging sequence, then again incorporating ± 0–1 random pixel shifts (constant over the entire image) between the different bands/looks. Next, the mis-registered images are registered using different interpolation schemes, assuming that the relative pixel offsets (or, equivalently, sensor motion), are known exactly. The two image cubes (control and registered/interpolated) are fed to the temperature retrieval algorithm and differenced in order to isolate the error in retrieved temperature due to registration alone.

For the input temperature scene, we used a calibrated brightness temperature map of the Bull Run coal-fired plant on Clinch River near Oak Ridge, Tennessee, acquired by band 11 (8.5–14 μm) of the Daedalus-1268 scanner (Fig. 3b). The temperature retrieved by the sensor with no included sensor jitter is shown in Fig. 3c. For the registration simulation, the imaging sequence was repeated multiple times including the random pixel shifts mentioned above. For each trial, registration temperature retrieval error was computed for the entire image. An example of the error in retrieved temperature due to registration is shown in Fig. 4a for one particular trial. A histogram of the errors computed for 40 trials is shown in Fig. 4b for three different interpolation algorithms, as well as for no registration. Printed at the top of the figure is the RMS error computed for each method. To reiterate, this figure represents the errors due to registration/interpolation alone assuming that the pointing information is known exactly. The histogram plot marked "None" thus represents the resulting temperature retrieval error due to interpolation when pointing knowledge is known only to within ± 1 pixel. The results show

that interpolation alone can be a significant source of error but can be minimized by using an interpolator which preserves the higher frequency content of the image.

3.3 Water Vapor Retrieval

3.3.1 Background

Atmospheric water vapor estimates are important products from remotely sensed data with applications in climate studies, weather forecasting, and also for performing atmospheric correction of other remote sensing data. There exist many techniques for retrieving total columnar water vapor. A relatively recent method is the application of differential absorption techniques to imaging spectrometry acquired from airborne instruments such as the Airborne Visible/Infrared Imaging Spectrometer (AVIRIS). This particular application is attractive due to both its ability to map atmospheric water vapor at high spatial resolution and also its capability to probe the lower atmosphere. Differential absorption techniques require taking ratios of images in different bands, both in and out of an absorption region. Thus, it is required to register the images in these bands prior to the retrieval; otherwise, any heterogeneity in the background reflectance will bias the result.

In this section, we investigate the errors in water vapor retrieval which are due to registration of the images used in the retrieval algorithm. In the first subsection, we simulate the problem by starting with a known water vapor map and an image of a vegetated surface to compute the effects of mis-registration and the resulting errors in the water vapor retrieval. In the second subsection, we apply the results to recent work using AVIRIS data to retrieve atmospheric water vapor.

3.3.2 Simulation

For the water vapor retrieval simulation, we used a differential absorption algorithm which is a simplification of the Continuum Interpolated Band Ratio (CIBR, Green et al., 1989). Briefly, this method takes ratios of channels in and out of the water vapor absorption band to compute the columnar atmospheric water vapor in between the sensor and the ground. The algorithm we used can be expressed by

$$\frac{L_m}{w_{r1}L_{r1} + w_{r2}L_{r2}} = \exp(-\alpha PW^{\beta}) \tag{3}$$

in which L_m is the measured radiance in the 940 nm water vapor absorption band (the "measurement" channel), L_{r1} and L_{r2} are the radiances measured in the two reference channels on either side of band m, w_{r1} and w_{r2} are weights, PW is the total columnar water vapor, and α and β are empirically determined constants (see Borel et al., 1996).

The simulation begins with a hypothetical water vapor map (Fig. 5a) and a near-infrared scene of the earth's surface (Fig. 5b), the latter of which is used for both reference channels $r1$ and $r2$. A vegetation scene was selected due to its high contrast in order to maximize the effects of mis-registration. Next, a simulated scene for channel m was computed from eqn. 3. All three channels are then "imaged" by neighborhood averaging over 10 by 10 pixel regions. To simulate the mis-registration during the sequence, channel m was imaged 10 separate times, shifting by 1 scene pixel in x and y each successive trial so that the mis-registration in the final image varied from 0–1 sensor pixel (1 sensor pixel = 10×10 scene pixels). This mis-registration was then removed (i.e., channel m was registered to $r1$ and $r2$) by removing the fractional pixel shifts using three different interpolation methods: nearest neighbor, bi-linear, and cubic convolution. Finally, the water vapor was retrieved using eqn. 3 on all 10 sets of registered channel m images. The error in retrieved water vapor was computed by differencing the values retrieved from interpolated scenes from the values acquired from images already initially registered.

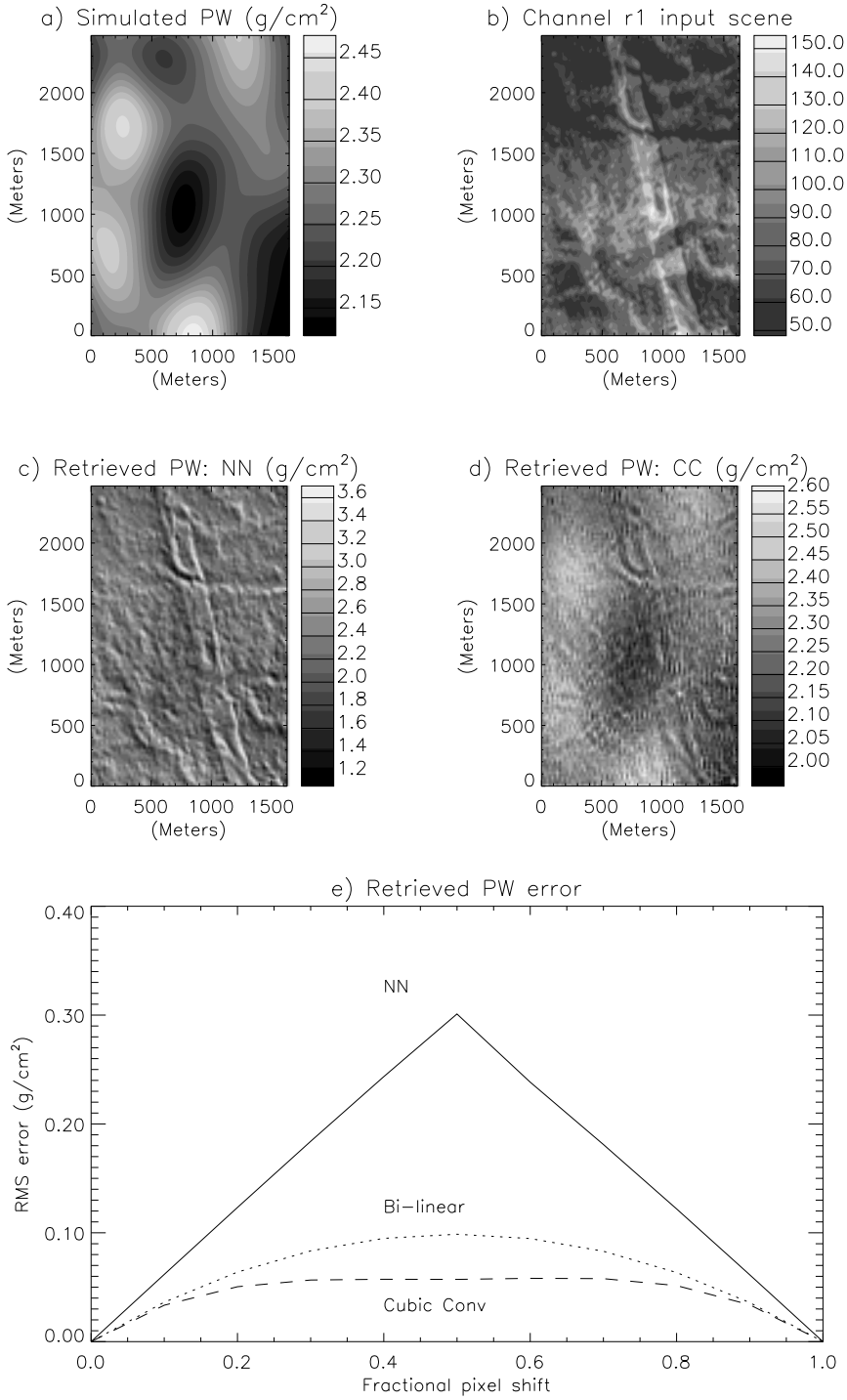

Figure 5: (a) Hypothetical water vapor map used in the simulation. (b) Near-IR input scene used for continuum channels $r1$ and $r2$. (c) Retrieved water vapor map computed using nearest neighbor interpolation, fractional pixel shift = 0.5. (d) Same as (c), but for cubic convolution ($\alpha = -1$). (e) Error in retrieved water vapor as a function of fractional pixel shift for the three different interpolation algorithms used in the simulation: nearest neighbor, bi-linear, and cubic convolution.

An example of the retrieved water vapor is shown in Fig. 5c for nearest neighbor registration, fractional pixel shift = 0.5 pixel. For a nearest neighbor algorithm, this figure represents the retrieved water vapor for a registration error of 0.5 pixel. Readily evident is the appearance of boundaries and other high-frequency content from the input scene. Not only have numerical errors been introduced into the computed water vapor values, but the 2-D texture of the actual water vapor distribution has been lost completely. Fig. 5d is identical to fig. 5c except that cubic convolution ($\alpha = -1$) was used for the interpolation. Many of the features from the input scene are still apparent, but the gross features from the original water vapor map can still be discerned. Fig. 5e shows the computed errors for all interpolation methods used for fractional pixel shifts 0–1 pixel. Note that the error in the retrieved water vapor is as high as 15% for a registration error of only 0.5 pixel. Not surprisingly, the error is minimized for the cubic convolution algorithm due to its better preservation of the higher frequencies.

3.3.3 Application to AVIRIS data

An example of the error due to mis-registration like that simulated above can be seen in recent data. Fig. 6 shows water vapor retrievals computed by Schläpfer et al. (1996) from 1995 AVIRIS data acquired near Oxnard, California. The first two panels show water vapor maps computed using different band-ratio techniques. The middle panel performed an additional correction by first removing the atmospheric path radiance. Note that in these two panels, the ground features are readily evident. In the third panel, a shift correction has been applied in order to register the channels used in the water vapor retrieval algorithm. This correction was necessary due to an amplifier problem in the AVIRIS focal plane which causes boundaries between light and dark areas to be somewhat delayed (see Schläpfer et al., 1996). Although this problem is not caused by mis-registration in the usual sense, it can be solved using the same techniques. Note that with the registration done properly, the boundaries between terrains have largely been removed so that the background reflectance no longer dominates the water vapor signal. As a result, much finer detail in the water vapor content can now be resolved.

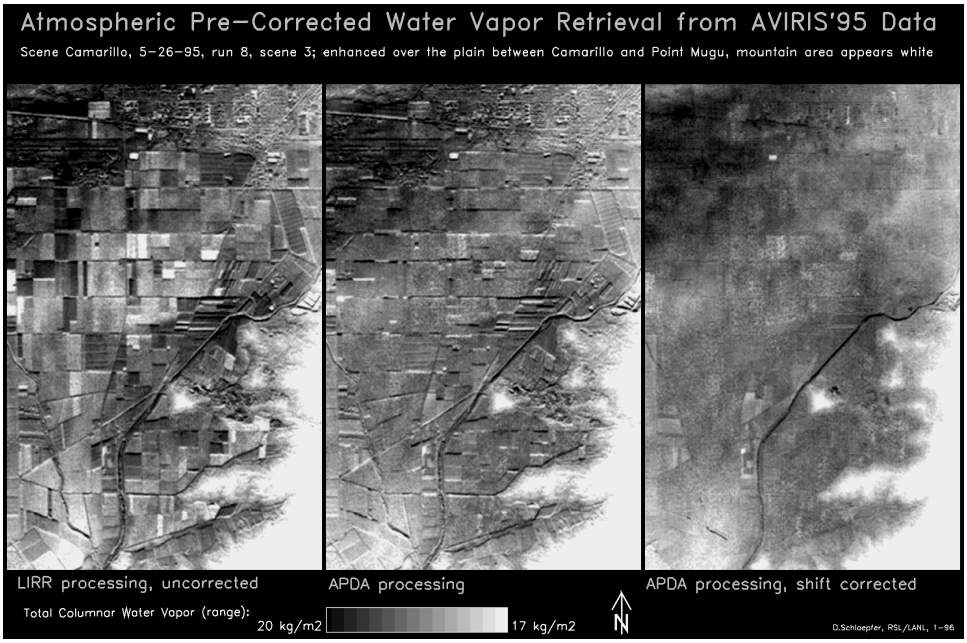

Figure 6: Water vapor retrievals from AVIRIS 1995 images near Oxnard, California, from Schläpfer et al., (1996). The leftmost panel is the retrieved water vapor map using a technique called the Linear Regression Ratio, or LIRR. The middle panel shows the retrieved water vapor using a technique called Atmospheric Pre-corrected Differential Absorption, or APDA, which corrects for atmospheric path radiance before computing the water vapor. The rightmost panel shows the APDA result with a shift correction applied to the data.

4 METHODS FOR DETERMINING SENSOR MOTION FOR REGISTRATION OF IMAGES ACQUIRED BY PUSHBROOM SCANNERS

4.1 Introduction

The utilization of multispectral imagery requires that the individual channels be registered (i.e., corresponding pixels in each band represent the same point on the ground), but doing so is not always straightforward. The methods used for registration seem to fall into two distinct categories: 1) "forward" methods which utilize known pointing information to give the orientation of the focal plane and thus the ground location of the pixels during imaging (Meyer, 1994; Reulke et al., 1994) and 2) image-based or "backwards" methods by which the spectral bands are correlated with each other on a region by region basis, and the offsets of maximum correlation, or, "lags," are used to shift and thus register all the images to each other.

We are currently interested in developing techniques for registering multispectral images acquired by a push-broom scanner. We are taking a novel approach and developing "hybrid" methods which use correlation analyses to determine spacecraft pointing or to refine any limited pointing knowledge which might be available. The improved pointing information can then be used to register all of the individual images. Here we present one method which might be used in this manner.

4.2 Baseline Correlation

Images acquired by a pushbroom scanner are built up one row at a time as a linear array of pixels is pushed across the scene. The spacing in the cross-track direction is determined by the pixel spacing in the focal plane, whereas the spacing in the along-track direction is determined by the ground track speed and the rate at which the pixels are read out. If the spacecraft is jittering during image acquisition, the cross-track location of the linear array will vary between readouts, and the along-track spacing will vary from row to row within the image. The distortion introduced by this motion makes registration of the different spectral bands more difficult.

Consider the m pixels in the n'th position of the linear arrays on a m-band multispectral pushbroom focal plane. Under ideal conditions, each of these pixels will image the same portion of the ground (i.e., lie on top of each other, but at slightly different times determined their spacing on the focal plane) during image acquisition (Fig. 7a). Under more realistic conditions, some unwanted jitter motion will exist during imaging that tends to scatter these pixels about that ground location where they should be (Fig. 7b). If the motion between bands is more or less uncorrelated (which depends upon the frequency content of the jitter and the spacing between channels on the focal plane), then a weighted average of all bands will yield a new image which is blurred, but has spacing proportional to the actual spacing on the ground so that the jitter motion has in effect been averaged out. This averaged image, or "baseline" (Fig. 7c), is then used a reference to which all bands are correlated line by line to extract spacecraft jitter motion as a function of time.

Fig. 8 shows results of the baseline correlation method. For the purposes of the simulation, we used night-time thermal imagery of the same scene shown in Fig. 3 using 5 bands in the mid- and long-wave IR. We first computed a hypothetical jitter motion time series, then used it to image the scene in all five bands. Next, the baseline was created in the manner described above, and the spacecraft motion was computed by correlating each band to the baseline, a few rows at a time. The true spacecraft motion is given by the solid line, whereas the computed motion is shown by the dotted line. Panels (a) and (b) are results for cross-track and along-track motion, respectively. The accuracy of this method should improve with the number of channels used in the creation of the baseline.

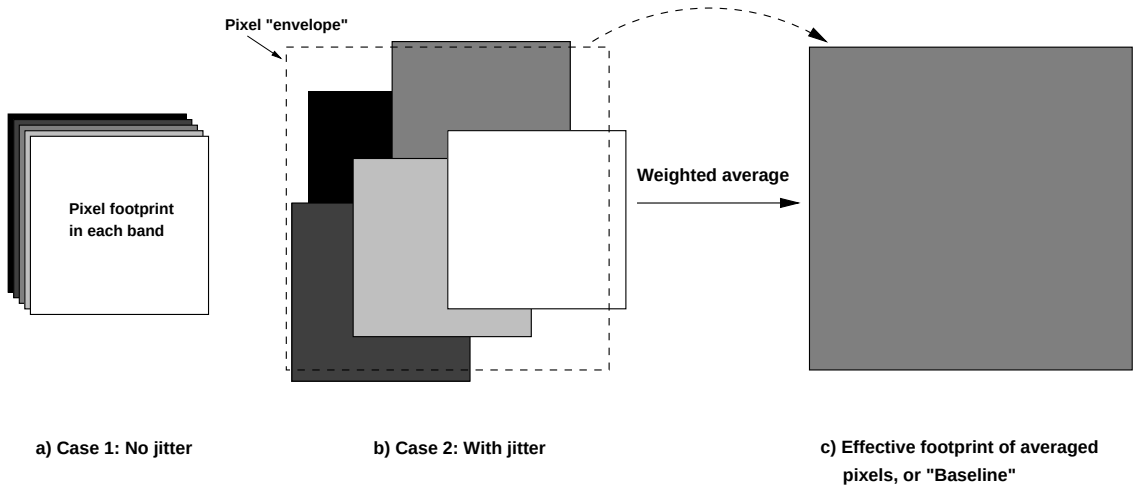

Figure 7: Idea behind "Baseline Correlation" method. (a) Corresponding pixels in different bands lie on top of each other when no jitter motion is present. (b) With jitter, those pixels are scattered about a mean position. (c) A weighted average of all the bands increases the effective pixel size but averages out the unwanted jitter motion. This "baseline" image can then be used a a reference to which all the other channels are correlated to determine spacecraft motion.

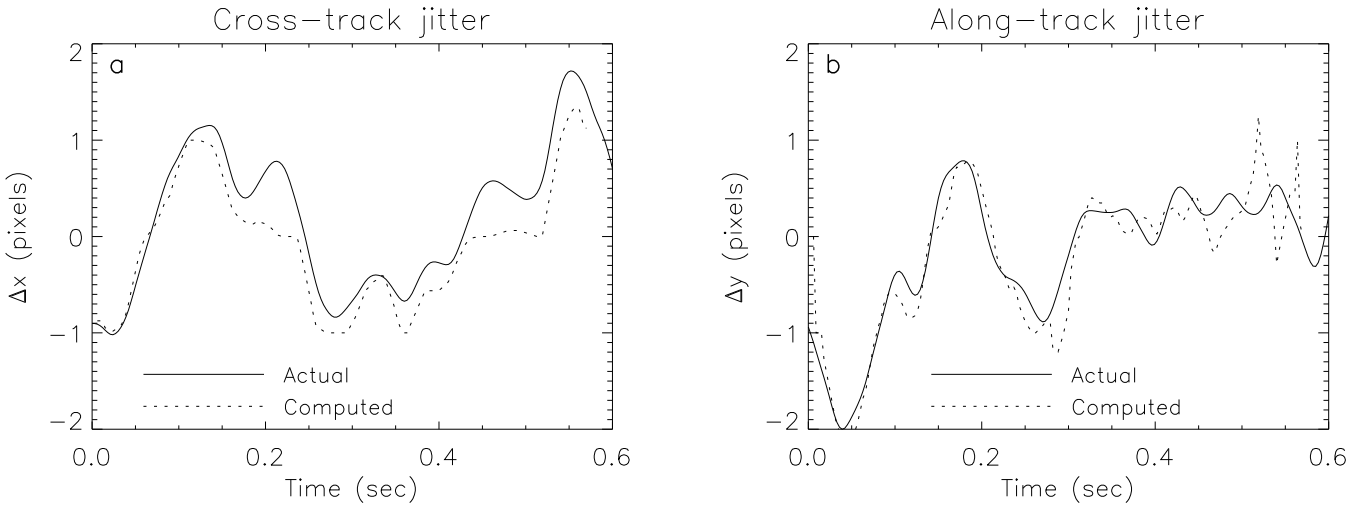

Figure 8: Results of the baseline correlation method for computing spacecraft jitter motion directly from imagery. (a) Cross-track results. (b) Along-track results. The actual motion is shown by the solid line, whereas the computed motion is given by the dotted line.

5 CONCLUSION

Exploiting the multispectral value of images acquired by whiskbroom and pushbroom scanners requires registration and interpolation, which degrades image quality. We have computed the MTF for different interpolation methods and have simulated the errors introduced by registration into physical quantities retrieved from multispectral imagery. Our results show that in complex retrievals utilizing multiple bands, registration and interpolation can introduce significant errors into retrieved quantities but can be minimized if registration is done properly using more accurate interpolation schemes. We have also presented a method which might be used to determine sensor platform motion for improved registration of multispectral images acquired by a pushbroom scanner.

6 REFERENCES

Berk, A., L. S. Bernstein, and D. C. Robertson, MODTRAN: A moderate resolution model for LOWTRAN 7, Report no. GL-TR-89-0122, Geophysics Laboratory, Air Force Systems Command, Hanscom AFB, MA, 1989.

Borel, C. C., W. B. Clodius, and J. Johnson, Water vapor retrieval over many surface types, *Proc. SPIE*, **2758**, in press, 1996.

Green, R. O., Carrére, V., and Conel, J. E., Measurement of atmospheric water vapor using the Airborne Visible/Infrared Imaging Spectrometer, Am. Soc. Photogram. and Remote Sensing, Workshop Image Processing, Sparkes, Nevada, 23–26 May, 1989.

Holst, G. C., *Electro-Optical Imaging System Performance*, JCD Publishing and SPIE Press, 1995.

McEwen, A., Lunar multispectral mosaics from Galileo's second Earth-Moon flyby (abstract), in *Lunar and Planetary Science XXIV*, 955–956, Lunar and Planetary Institute, Houston, 1993.

Park, S. K., and R. A. Schowengerdt, Image reconstruction by parametric cubic convolution, *Computer Vision, Graphics, and Image Processing*, **23**, 258–272, 1983.

Reulke, R., N. Reulke, and H. Jahn, Numerical simulation system for generation of image data from spaceborne imaging sensors for planetary exploration, *Proc. SPIE*, **2318**, 144–154, 1994.

Schläpfer, D., C. C. Borel, J. Keller, and K. Itten, Atmospheric pre-corrected differential absorption techniques to retrieve columnar water vapor: Application to AVIRIS 91/95 data, *Proc. 6th JPL Airborne Earth Science Workshop*, in press, 1996.

Smith, B. W., C. C. Borel, W. B. Clodius, B. E. Laubscher, and P. G. Weber, End-to-end performance modeling of passive remote sensing systems, *Proc. SPIE*, **2743**, in press, 1996.

Tornow, C., C. C. Borel, and B. J. Powers, Robust water temperature retrieval using multi-spectral and multi-angular IR measurements, *Proc. IGARSS '94*, 441–443, 1994.